# An Innovative Optimization Strategy for Tiling Orthogonal Polygon Apertures

**P. Rocca, N. Anselmi, A. Polo, and A. Massa**

# Contents

# 1 Introduction

This work presents an innovative tiling optimization strategy for arbitrary orthogonal-polygon shaped apertures. An exhaustive search approach, together with a multi-objective strategy, has been used in order to obtain optimal tiling configurations, jointly optimizing two different pattern features of interest. A simple example validating the proposed method has been finally reported.

# 2 Mathematical Formulation

## 2.1 Tilig Definitons and Theorems

### 2.1.1 Orthogonal Polygons

A polygon is called *orthogonal* (or *rectilinear*) if its edges are either horizontal or vertical (i.e., if edges meet at right angles)

Let us consider a set $\mathcal{L}$ of $M \times N$ pixels:

- the pixel-vertices, **v**=$\{v_{mn}; m = 0, ..., M; n = 0, ..., N\}$;
- the pixel-edges, **e**=$\{e_{mn \to m(n\pm1)}, e_{mn \to (m\pm1)n}; m = 0, ..., M-1; n = 0, ..., N-1\}$.

An orthogonal polygon $\mathcal{P}$ composed by $P$ contiguous pixels is defined as a subset of $\mathcal{L}$ as:

$$\mathcal{P} = \{\mathbf{R}, \partial\mathbf{R}\} \tag{1}$$

where

- $\mathbf{R} = \left\{v_{mn}\delta_{mn}^{(p)}, m = 0, ..., M-1, n = 0, ..., N-1, p = 1, ..., P\right\}$is the set of $P$ pixel vertices that belongs to $\mathcal{P}$, being $\delta_{mn}^{(p)}$ the Dirac function: $\delta_{mn}^{(p)} = 1$ if the $mn$-th vertice belongs to $\mathcal{P}$, $\delta_{mn}^{(p)} = 0$ otherwise;
- $\partial\mathbf{R} = \left\{e_{b\to(b+1)}, b = 1, ..., B\right\}$is the set of $B$ boundary edges of the polygon $\mathcal{P}$.

.

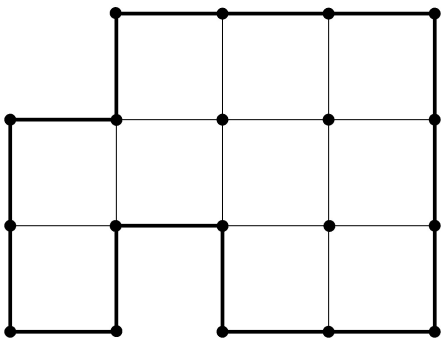

Figure 1: Example of orthogonal (rectilinear) polygon.

### 2.1.2 Height Function

Following the guidelines reported, The height function $h(\cdot)$ is defined on the pixel-vertices while the $h$-values are determined by considering the pixel-edges. Towards this end, the aperture pixels are colored according to a black, $\zeta_{mn} = -1$, and white, $\zeta_{mn} = 1$, checkerboard pattern, starting with an arbitrary color for the first pixel $\zeta_{11} = \pm 1$ (e.g., $\zeta_{11} = 1$ in Figs. 2-3), and the edges of white/black pixels are oriented clockwise/counterclockwise (Fig. 2). Then, the following procedure is used:

- With reference to a clustered configuration $\mathbf{c}^{(t)}$ of tile shapes vertically or horizontally oriented (e.g., Fig. 4), select an internal vertex $v_{mn}^{(t)} \in \mathbf{v}_{int}^{(t)}$ with at least one neighboring vertex, denoted as $v_{pg}^{(t)} \in \overline{\mathbf{v}}_{mn}^{(t)}$ [$\overline{\mathbf{v}}_{mn}^{(t)} = \{v_{(m-1)n}^{(t)}$, $v_{(m+1)n}^{(t)}$, $v_{m(n-1)}^{(t)}$, $v_{m(n+1)}^{(t)}\}$ being the set of vertices neighbor to $v_{mn}^{(t)}$], having the height function value, $h_{pg}^{(t)} = h\left(v_{pg}^{(t)}\right)$ already set (i.e., $v_{pg}^{(t)} = v_{(m-1)n}^{(t)}$ or $v_{pg}^{(t)} = v_{(m+1)n}^{(t)}$ or $v_{pg}^{(t)} = v_{m(n-1)}^{(t)}$ [e.g., Fig. 4(*b*) and Fig. 4(*d*)] or $v_{pg}^{(t)} = v_{m(n+1)}^{(t)}$ [e.g., Fig. 4(*a*) and Fig. 4(*c*)]). Then, determine the unknown value $h_{mn}^{(t)}$ according to one of the following "*tiling rules*":

  - if the edge $e_{mn \to pg}$ is directed from $v_{mn}^{(t)}$ to $v_{pg}^{(t)}$ in the black-and-white checkerboard and it belongs to the contour of a domino tile of $\mathbf{c}^{(t)}$ [Fig. 4(*a*)] then $h_{mn}^{(t)} = h_{pg}^{(t)} - 1$;
  - if the edge $e_{mn \to pg}$ is directed from $v_{pg}^{(t)}$ to $v_{mn}^{(t)}$ in the black-and-white checkerboard and it belongs to the contour of a domino tile of $\mathbf{c}^{(t)}$ [Fig. 4(*b*)] then $h_{mn}^{(t)} = h_{pg}^{(t)} + 1$;
  - if the edge $e_{mn \to pg}$ is directed from $v_{pg}^{(t)}$ to $v_{mn}^{(t)}$ in the black-and-white checkerboard and it does not belong to the contour of a domino tile of $\mathbf{c}^{(t)}$ [Fig. 4(*c*)] then $h_{mn}^{(t)} = h_{pg}^{(t)} - 3$;
  - if the edge $e_{mn \to pg}$ is directed from $v_{mn}^{(t)}$ to $v_{pg}^{(t)}$ in the black-and-white checkerboard and it does not belong to the contour of a domino tile of $\mathbf{c}^{(t)}$ [Fig. 4(*d*)] then $h_{mn}^{(t)} = h_{pg}^{(t)} + 3$;

  Iterate the process for all the internal vertices, $v_{mn}^{(t)} \in \mathbf{v}_{int}^{(t)}$, $m = 1, ..., M-1$; $n = 1, ..., N-1$ [Fig. 4(*e*)].

### 2.1.3 Thurston Theorem

Thurston presents an algorithm that allows to prove the tilability of a simply connected region. We can thus formulate the following theorem:

> **Thurston Theorem**: Let $R$ be a simply connected region in the plane, and let $n = |R|$ be the area of $R$. There exists an algorithm that decides tileability of $R$ in time $O(n \log n)$.

### 2.1.4 Thurston Algorithm

Given a region $R$, there exist a "minimal" tiling, i.e the tiling whose height function has no local maximum except on the boundary of $R$.

Thurston derived a linear algorithm which construct the "minimal" tiling of $R$, or proves that $R$ is not tilable:

- **INPUT**: a region $R$
- **OUTPUT**: the "minimal" tiling of $R$ if $R$ is tilable, *untilability* otherwise.

1. Initialize a list $T$ containing the tiles and the positions of the tiles (i.e a tiling of $R$), to an empty set.
2. If $R$ is a single point,
   - **RETURN** $T$
3. Compute the height function on the boundary of $R$. If a vertex is given two different heights,
   - **RETURN** $R$ is untilable.
4. Select the lattice point of $\partial R$ with maximum height.
5. There exist two lattice points $u, w \in \partial R$ such that $(u, v)$ and $(v, w)$ are edges of $\partial R$ . Place a tile $\tau$ on $R$ so that $u, v, w \in \tau$.
6. Add $\tau$ and its position to $T$.
7. Update $R$ to $R/\tau$ (i.e. subtract the tile $\tau$ from the region $R$) and go to 2.

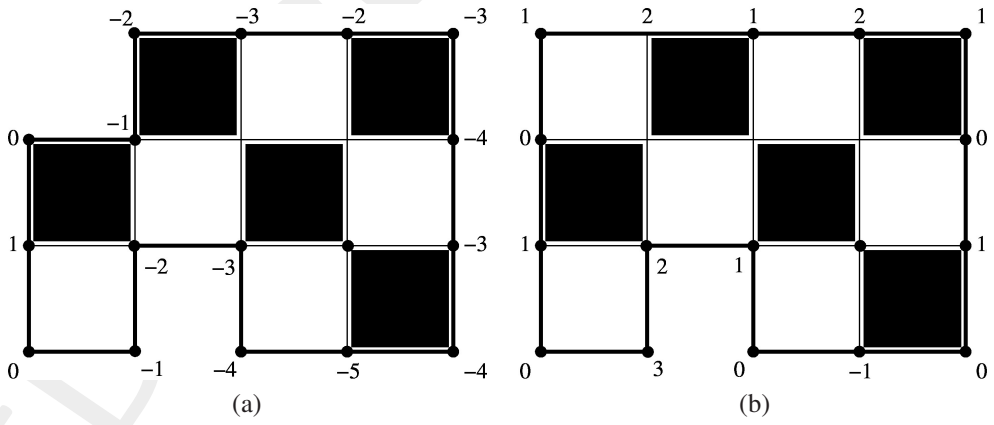


Figure 2: Example of tilable (a) and non-tilable (b) orthogonal polygon by dominoes, exploiting the Thurston Theorem

### 2.1.5 Tilability Theorem

Given an orthogonal polygon shaped aperture $\mathcal{O}$, there exists a way to understand if the apertures tilable or not. The method is based on the height function introduced, and used for the domino tiled synthesis method of rectangular shaped arrays, generalized in this work for arbitrarly orthogonal polygon shaped apertures. More in detail the tilability condition is

given from the knowledge of the height function defined over the vertices of the boundary of $\mathcal{O}$, $\partial\mathcal{O} = \{b_s;\ s = 1, ..., S\}$ and by applying the tilability theorem. The height function *on the boundary* of $\mathcal{O}$, $h(b_s)$, $s = 1, ..., S$, are computed as

$$h(b_s) = \begin{cases} h(b_{s-1}) + 1\ if\ \ (b_{s-1} \rightarrow b_s) \in \mathcal{W} \\ h(b_{s-1}) - 1\ if\ \ (b_{s-1} \rightarrow b_s) \in \mathcal{B} \end{cases} \tag{2}$$

where the notation $v_s \rightarrow v_t$ is used to refer to an oriented edge connecting a pair of adjacent vertices$(v_s, v_t) \in \mathcal{O}$, and $\mathcal{W}$ and $\mathcal{B}$ being the set of edges oriented clockwise/counter-clockwise, around a white/black cell. Consequently, a directed graph $G$ can be associated to the aperture $\mathcal{O}$ according to the chessboard-like pattern. Moreover, an auxiliary function $g(b_s)$ $s = 1, ..., S$ is her

$$g(b_s) = \min_{b_i \in \partial\mathcal{O}} \left[h(b_i) + \Delta(b_s, b_i)\right],\ s = 1, ..., S \tag{3}$$

where $\Delta(b_i, b_s)$ is the minimum number of edges that are necessary to reach $b_i$ from $b_s$ in $G$. Once obtained $h(b_s)$ and $g(b_s)$, $s = 1, ..., S$ the tilability of $\mathcal{O}$ by domino-like tiles is given by the following theorem

**Theorem**: Given an orthogonal polygon $\mathcal{O}$ composed by $P$ cells defined over a regular square grid, and the corresponding $h(b_s)$ and $g(b_s)$, $s = 1, ..., S$, functions, $\mathcal{O}$ is tilable by $P/2$ domino-lke tiles grouping 2 cells sharing one edge if and only if the following condition holds

$$h(b_s) = g(b_s),\ s = 1, ..., S \tag{4}$$

### 2.1.6 Cardinality of the Solution Space

For orthogonal polygon shaped apertures, for the best of the authors knoledge, there still not exist any analytic formula or theorem giving the exact number of the total admissible domino tilings $\Gamma$. In this section some reliable bounds on $\Gamma$ are provided, exploiting the analytic formula for counting the tilings of an $M \times N$ rectangular region:

$$T(M,N) = 2^{\frac{MN}{2}} \prod_{m=1}^{M} \prod_{n=1}^{N} \left[ cos^2\left(\frac{\pi m}{M+1}\right) + cos^2\left(\frac{\pi n}{N+1}\right) \right]^{1/4} \tag{5}$$

The proposed bounds are obtained as follows:

- the upper bound $\overline{\Gamma}$ is obtained as

$$T\left(\overline{M},\overline{N}\right) - \sum_{i=1}^{I} T\left(\overline{M}_i,\overline{N}_i\right) \tag{6}$$

  , being $\overline{M}$ and $\overline{N}$ the edge of the smallest rectangle inscribing the orthogonal polygon and $T\left(\overline{M}_i,\overline{N}_i\right)$, $i = 1, ..., I$ the number of tiling of $I$ rectangles obtained as intersection of $P$ and the $\overline{M} \times \overline{N}$ rectangle;

- the lower bound $\underline{\Gamma}$ is obtained as

$$\prod_{i=1}^{I} T\left(\underline{M}_i,\underline{N}_i\right) \tag{7}$$

  , being $T\left(\underline{M}_i,\underline{N}_i\right)$, $i = 1, ..., I$ the number of tiling of $I$ rectangles, covering, without overlapping, the orthogonal polygon.

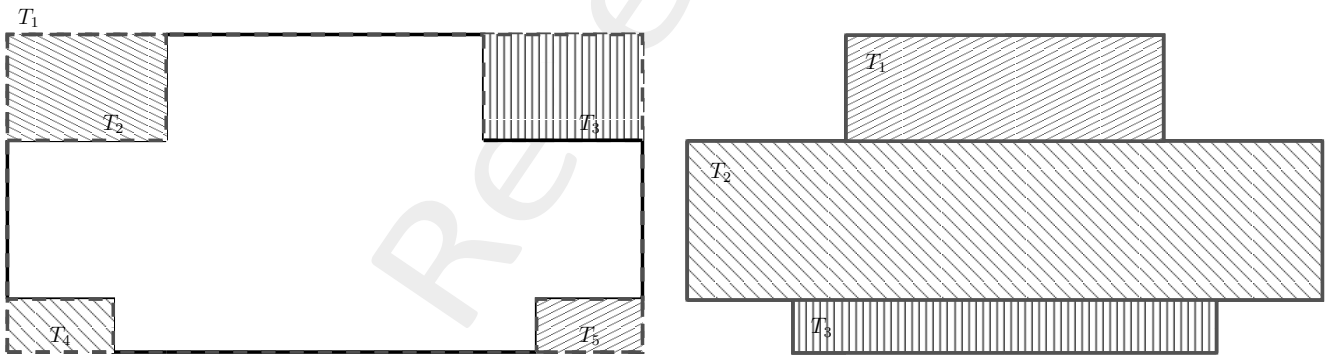


(a) (b)

Figure 3: Example of upper $\overline{\Gamma}$ (a) and lower bound $\underline{\Gamma}$ (b) orthogonal polygon by dominoes, exploiting the cardinality theorem for rectangular regions.

## 2.2 Mult-Objective Problem Formulation

**Multi Objective Problem (*MOP*)**

$$\min_{\mathbf{c}} \left[\mathbf{\Phi}(\mathbf{c})\right] \quad s.t. \;\; \mathbf{c} \in \Omega \tag{8}$$

where $\Omega$ is the feasible space of the unknowns and

$$\mathbf{\Phi}(\mathbf{c}) = \{\Phi_r;\, r = 1, ..., R\}$$

**Pareto Dominance**

Given two solutions $\mathbf{c}_1 \in \Omega$ and $\mathbf{c}_2 \in \Omega$ of (8), $\mathbf{c}_1 \preceq \mathbf{c}_2$ (i.e. $\mathbf{c}_1$ dominates $\mathbf{c}_2$) if $\Phi_r(\mathbf{c}_1) \leq \Phi_r(\mathbf{c}_2)$, $r = 1, ..., R$.

**Pareto Set (*PS*)**

The Pareto set (*PS*) of (8) is the set of non dominated solutions, defined as

$$PS = \{\mathbf{c} \in \Omega : \nexists \mathbf{c}' \in \Omega \, s.t. \, \mathbf{c}' \preceq \mathbf{c}\} \tag{9}$$

**Pareto Front (*PF*)**

The pareto front is the image of *PS* considering as mapping function the objectives cost-functions $\Phi_r$, $r = 1, ..., R$:

$$PF = \{\Phi_r(\mathbf{c}), \, \mathbf{c} \in PS, \, r = 1, ..., R\} \tag{10}$$

**Normalized Pareto Front (*NPF*)**

The normalized Pareto Front (*NPF*) is defined as

$$NPF = \left\{\widehat{\Phi}_r(\mathbf{c}) = \frac{\Phi_r(\mathbf{c})}{L_r}; \, \mathbf{c} \in PS, \, r = 1, ..., R\right\} \tag{11}$$

where

$$L_r = \max_{\mathbf{c} \in PS} [\Phi_r(\mathbf{c})] - \min_{\mathbf{c} \in PS} [\Phi_r(\mathbf{c})]$$

## 2.3 Multi-Objective Optimization of Phased Array Tilings

Let us consider a planar array of P elements, placed over the xy-plane, within an aperture $A$ with orthogonal-polygon shape (i.e. a polygon in which every edge is either horizontal or vertical). The isotropic radiating elements are located at the cells barycenter of a rectangular lattice, uniformly spaced by $d_x$and $d_y$ along the $x-$axis and $y-$axis respectively. The set of domino tiles $\mathcal{T} = \{\tau_1, \tau_2\}$, $\tau_1$ being the vertical domino, and $\tau_2$ the horizontal domino, are considered. Accordingly, the arising power pattern is computed as:

$$P(u, v) = \left| \sum_{p=1}^{P} w_p e^{j \frac{2\pi}{\lambda}(x_p u + y_p u)} \right|^2 \tag{12}$$

where in (12) $\lambda$ is the wavelength, $u = sin\theta cos\phi$ and $v = sin\theta sin\phi$ are the direction cosines, while $x_p$, $y_p$ is the p-th element position coordinates. The equivalent element excitation $w_p, p = 1, ..., P$ is the weigth associated to the p-th element and is equal to the complex coefficient of the T/R module connected to the tile's output port, obtained as:

$$w_p = \frac{1}{N_T} \sum_{q=1}^{Q} \sum_{i=1}^{P} \alpha_q e^{j\beta_q} \delta_{c_p}^{(q)}, \; p = 1, ..., P \tag{13}$$

where in (13) $x_q$ and $y_q$, $q = 1, ..., Q$ are the tiles barycenters, $(u_s, v_s)$ is the beam steering direction, $N_T$ is the number of elements grouped by a single tile, $\underline{c} = \{c_p \in [1, Q], \, p = 1, ..., P\}$ is the set of integers numbers defining the tiling

partitioning, $\delta_{c_p}^{(q)}$ is the Kroneker delta function which is equal to$\delta_{c_p}^{(q)} = 1$ if $c_p = q$ (i.e. the $p-$th element belongs to the $q-$th tile), otherwise $\delta_{c_p}^{(q)} = 0$ , and finally $\alpha_p$, $p = 1, ..., P$ and $\beta_p$, $p = 1, ..., P$ are tiles amplitude and phase coefficients, respectively. Accordingly to the above formulation, the following multi-objective optimization problem ($MOP$) is addressed:

*Multi-Objective Optimization of Arbitrary Shaped Phased Arrays* - given an array of arbitrary aperture, with elements positioned over a rectangular lattice, and two domino-like tiles $\left(\sigma^V, \sigma^H\right)$, find the optimal tiling/clustering configuration $\mathbf{c}^{opt}$ and the corresponding sub-array weights $\boldsymbol{\alpha}^{opt}$and $\boldsymbol{\beta}^{opt}$, such that the radiated pattern jointly fits multiple user-defined requirements $\Phi_r\left(\mathbf{c}; \boldsymbol{\alpha}, \boldsymbol{\beta}\right)$, $r = 1, ..., R$, with the man lobe steered toward $(\theta_0, \phi_0)$.

In order to comply with multiple and conflicting objectives, a set of Pareto optimal solutions will be provided to the designer who is allowed to choose the best solution according to user-defined criterion. The set of Pareto optimal solutions are obtained as:

$$\left(\mathbf{c}^{opt}; \boldsymbol{\alpha}^{opt}, \boldsymbol{\beta}^{opt}\right) = \arg\left[\min_{\mathbf{c};\boldsymbol{\alpha},\boldsymbol{\beta}} \left\{ \begin{array}{c} \Phi_1\left(\mathbf{c}; \boldsymbol{\alpha}, \boldsymbol{\beta}\right) \\ \vdots \\ \Phi_R\left(\mathbf{c}; \boldsymbol{\alpha}, \boldsymbol{\beta}\right) \end{array} \right\}\right] \tag{14}$$

Due to the high computational burden, required by a state of the art $MOP$ strategy,the amplitude and phase excitation cefficients of the sub-array outputs are analyically obtained, according to the tiling configuration $\underline{c}$:

$$\alpha_q^{EM} = \frac{1}{2}\sum_{p=1}^{P} \alpha_p^{ref} \delta_{c_p}^{(q)},\ q = 1, ..., Q \tag{15}$$

$$\beta_q^{EM} = \frac{1}{2}\sum_{p=1}^{P} \beta_p^{ref} \delta_{c_p}^{(q)},\ q = 1, ..., Q \tag{16}$$

being $\alpha_p^{ref}$, $p = 1, ..., P$ and $\beta_p^{ref}$, $p = 1, ..., P$ a set of reference amplitude and phase excitations. In order to assure the optimality of the solutions provided by the $MOP$ strategy, the reference excitations are obtained by means of a convex programming optimization, yelding optimal amplitude and phase coefficients of the fully-populated reference array, satisfying some user defined constraints on the radiation pattern, and maximizing the directivity in the beam pointing direction. The constraints are defined through a power mask $M\left(u, v\right)$, whose profile arbitrarly shapes the maximum allowed power levels in each angular direction.

Accordingly the following objectives, are considered:

$$\Phi_1\left(\underline{c}\right) = \int_{-1}^{1}\int_{-1}^{1} \left[M\left(u, v\right) - P\left(u, v; \underline{c}\right)\right] \mathcal{H}\left[P\left(u, v; \underline{c}\right) - M\left(u, v\right)\right] dudv$$

$$\Phi_2\left(\underline{c}\right) = D\left\{P\left(u, v; \underline{c}\right)\right\}$$

$$\Phi_3\left(\underline{c}\right) = SLL\left\{P\left(u,v;\underline{c}\right)\right\}$$

$$\Phi_4\left(\underline{c}\right) = HPBW_{AZ}\left\{P\left(u,v;\underline{c}\right)\right\}$$

$$\Phi_5\left(\underline{c}\right) = HPBW_{EL}\left\{P\left(u,v;\underline{c}\right)\right\}$$

Once the tiling solutions have been exhaustively obtained, the $N$ objectives are evaluated for each tiling. The optimal solution are chosed among the pareto-optimal subset, i.e. the set of solutions that are non- dominated by others in terms of the $N$ objectives.

# 3 Numerical Results

## 3.1 Rectangle 5x8

**Array Analysis Parameters:**

- Total Number of Elements: $P = 40$
- Spacing: $d = \lambda/2$
- Number of Samples along $u$: $512$
- Number of Samples along $v$: $512$
- Steering $\theta$ Direction: $\theta_s = 0$
- Steering $\phi$ Direction: $\phi_s = 0$
- Tapering: Dolph $SLL = -20$ [dB]

**Tiling Parameters:**

- Tile: Domino
- Number of Elements in each Tile: $N_T = 2$
- Total Number of Configurations: $\Gamma = 14824$
- Number of Inner Lattice Points: $N_{inn} = 28$

**Objectives:**

- $OBJ^{(1)} = SLL$
- $OBJ^{(2)} = HPBW_{AZ}$
- $OBJ^{(3)} = HPBW_{EL}$

**STATE OF THE ART - SOP (ETM/GA Approach)**

**Genetic Algorithm Parameters:**

- Number of Unknowns: $N_u = 56$
- Population Dimension: $U = 8$
- Number of Iterations: $I = 100$
- Number of Fitness Evaluations: $N_{FE} = 800$
- Crossover Probability: $p_{cross} = 0.9$
- Mutation Probability: $p_{mut} = 0.01$
- Diversity Percentage: $p_{div} = 10\%$
- Cost Function $\Phi\left(t\right) = OBJ^{(1)}$

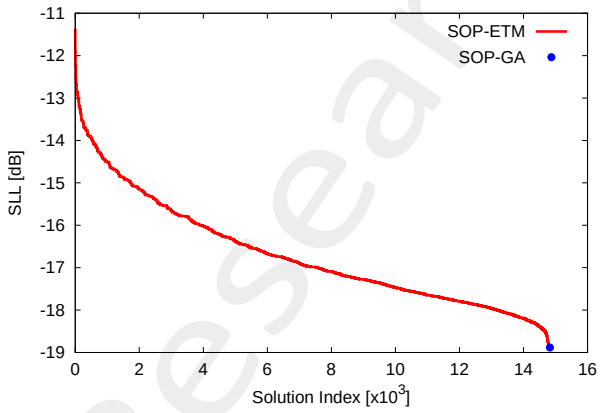


Figure 4: Pareto front of the $ETM$ and $GA$ soutions considering: $OBJ^{(1)} = SLL$ (SOP).

**RESULTS - SOP (ETM)**

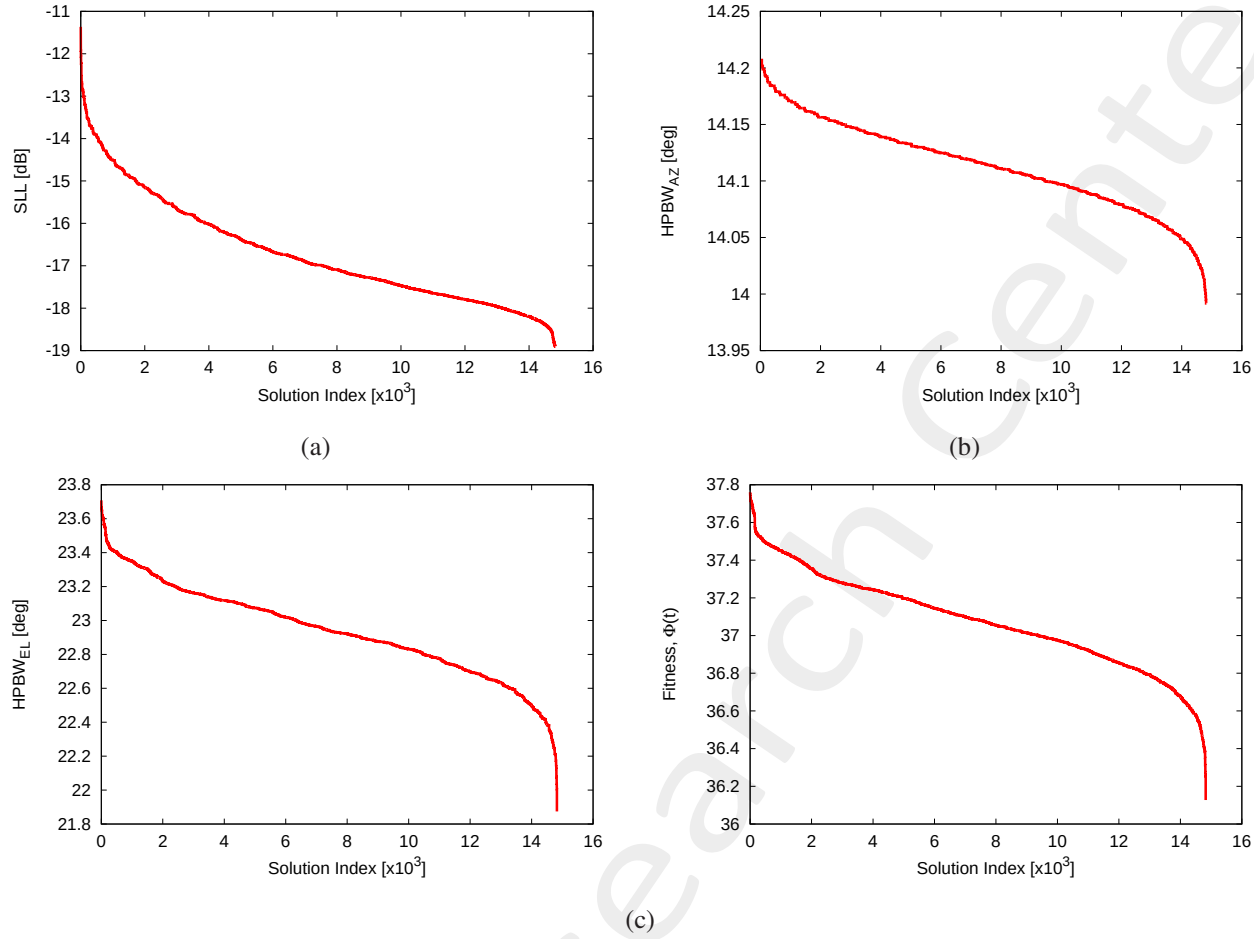


Figure 5: Pareto front of the $ETM$ soutions considering: $OBJ^{(1)} = SLL$ vs $OBJ^{(2)} = HPBW_{AZ}$ (a), $OBJ^{(1)} = SLL$ vs $OBJ^{(3)} = HPBW_{EL}$(b), $OBJ^{(2)} = HPBW_{AZ}$ vs $OBJ^{(3)} = HPBW_{EL}$(c).

- The optimal tilings optimizing $OBJ^{(1)}$are: 3223, 186, 1267, 9323
- The optimal tilings optimizing $OBJ^{(2)}$are: 27, 44, 47, 231, 234, 4659, 12750, 14065, 14069, 14752, 14756, 14787
- The optimal tilings optimizing $OBJ^{(3)}$are: 11729
- The optimal tilings optimizinf the fitness function $\Phi\left(t\right) = OBJ^{(1)} + OBJ^{(2)} + OBJ^{(3)}$are: 11729

**RESULTS - Pareto Fronts (ETM)**

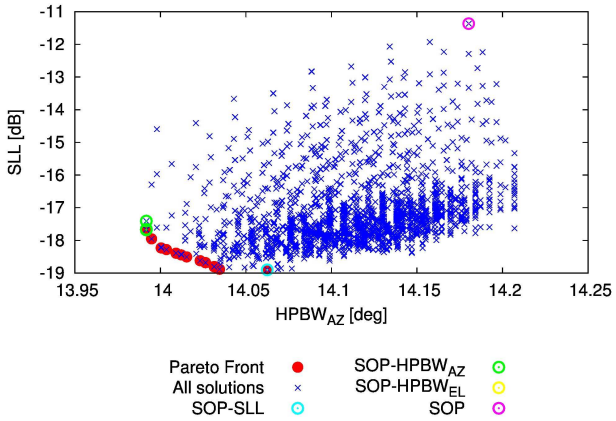


(a)

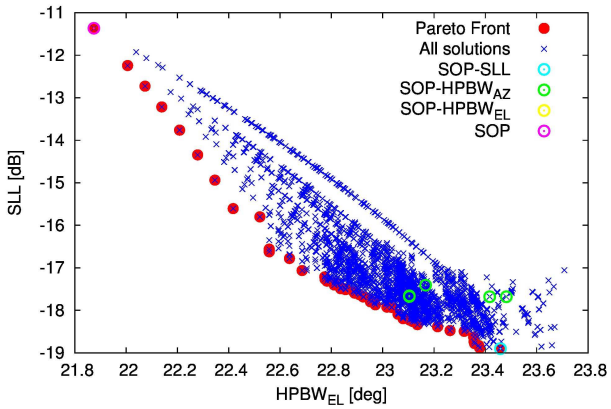


(b)

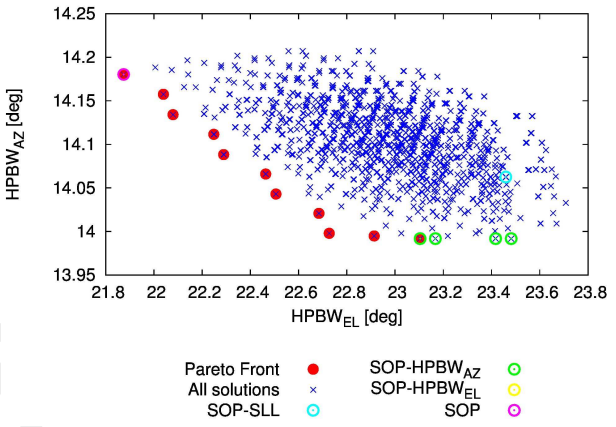


(c)

Figure 6: Pareto front of the $ETM$ soutions considering: $OBJ^{(1)} = SLL$ vs $OBJ^{(2)} = HPBW_{AZ}$ (a), $OBJ^{(1)} = SLL$ vs $OBJ^{(3)} = HPBW_{EL}$(b), $OBJ^{(2)} = HPBW_{AZ}$ vs $OBJ^{(3)} = HPBW_{EL}$(c).

**RESULTS - Pareto Fronts (MOP)**

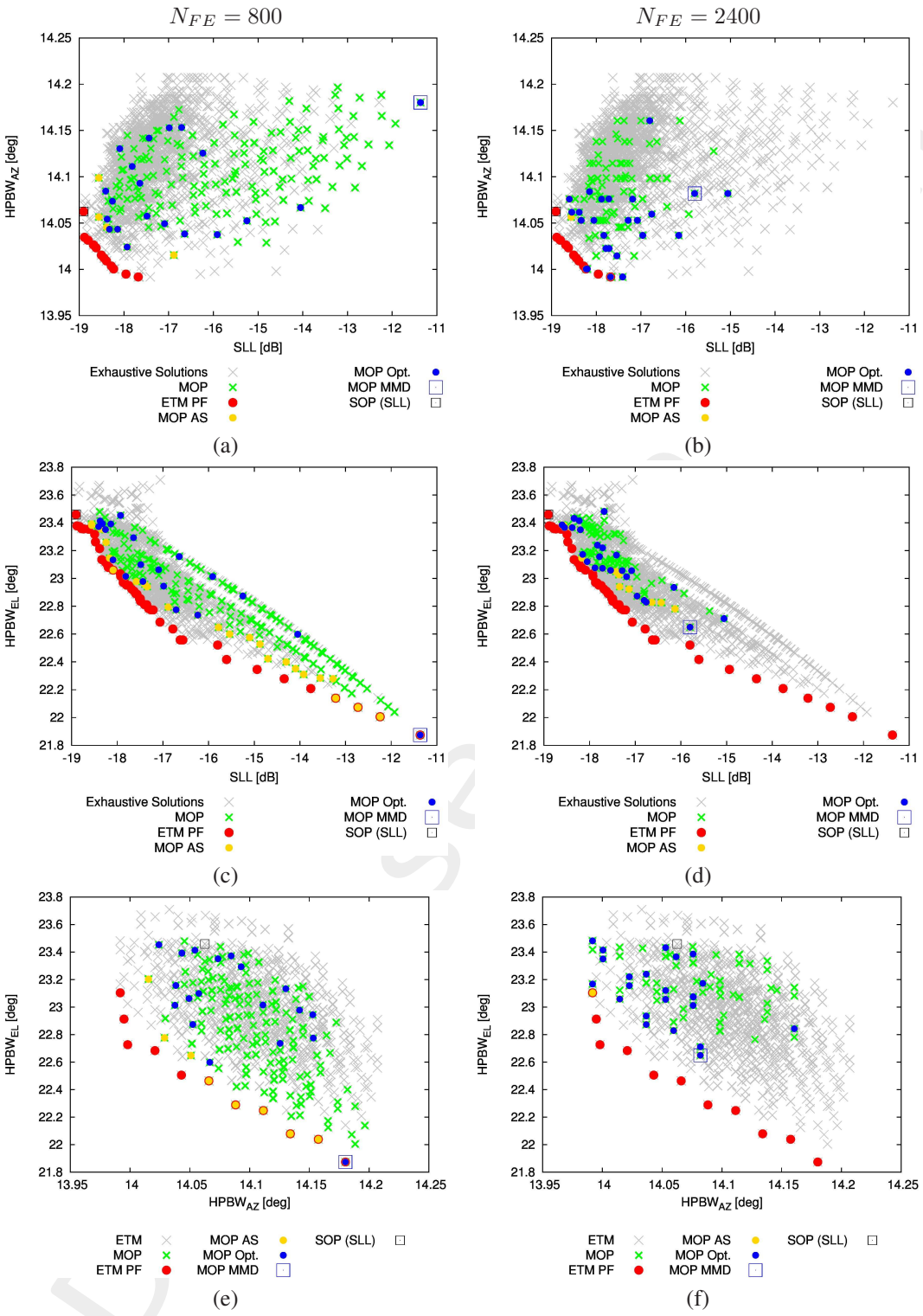


Figure 7: Exhaustive Pareto front as compared to the $MOP$ Approximation Set considering: $OBJ^{(1)} = SLL$ vs $OBJ^{(2)} = HPBW_{AZ}$ (a)(b), $OBJ^{(1)} = SLL$ vs $OBJ^{(3)} = HPBW_{EL}$(c)(d), $OBJ^{(2)} = HPBW_{AZ}$ vs $OBJ^{(3)} = HPBW_{EL}$(e)(f), for $N_{FE} = 800$ and $N_{FE} = 2400$ fitness evaluations.

## 3.2 Rectangle 8x8

**Array Analysis Parameters:**

- Total Number of Elements: $P = 64$
- Spacing: $d = \lambda/2$
- Number of Samples along $u$: $512$
- Number of Samples along $v$: $512$
- Steering $\theta$ Direction: $\theta_s = 0$
- Steering $\phi$ Direction: $\phi_s = 0$
- Tapering: Dolph $SLL = -20$ [dB]

**Tiling Parameters:**

- Tile: Domino
- Number of Elements in each Tile: $N_T = 2$
- Total Number of Configurations: $\Gamma = 12989 \times 10^7$
- Number of Inner Lattice Points: $N_{inn} = 49$

**Objectives:**

- $OBJ^{(1)} = SLL$
- $OBJ^{(2)} = HPBW_{AZ}$
- $OBJ^{(3)} = HPBW_{EL}$

**RESULTS - Pareto Fronts (MOP)**

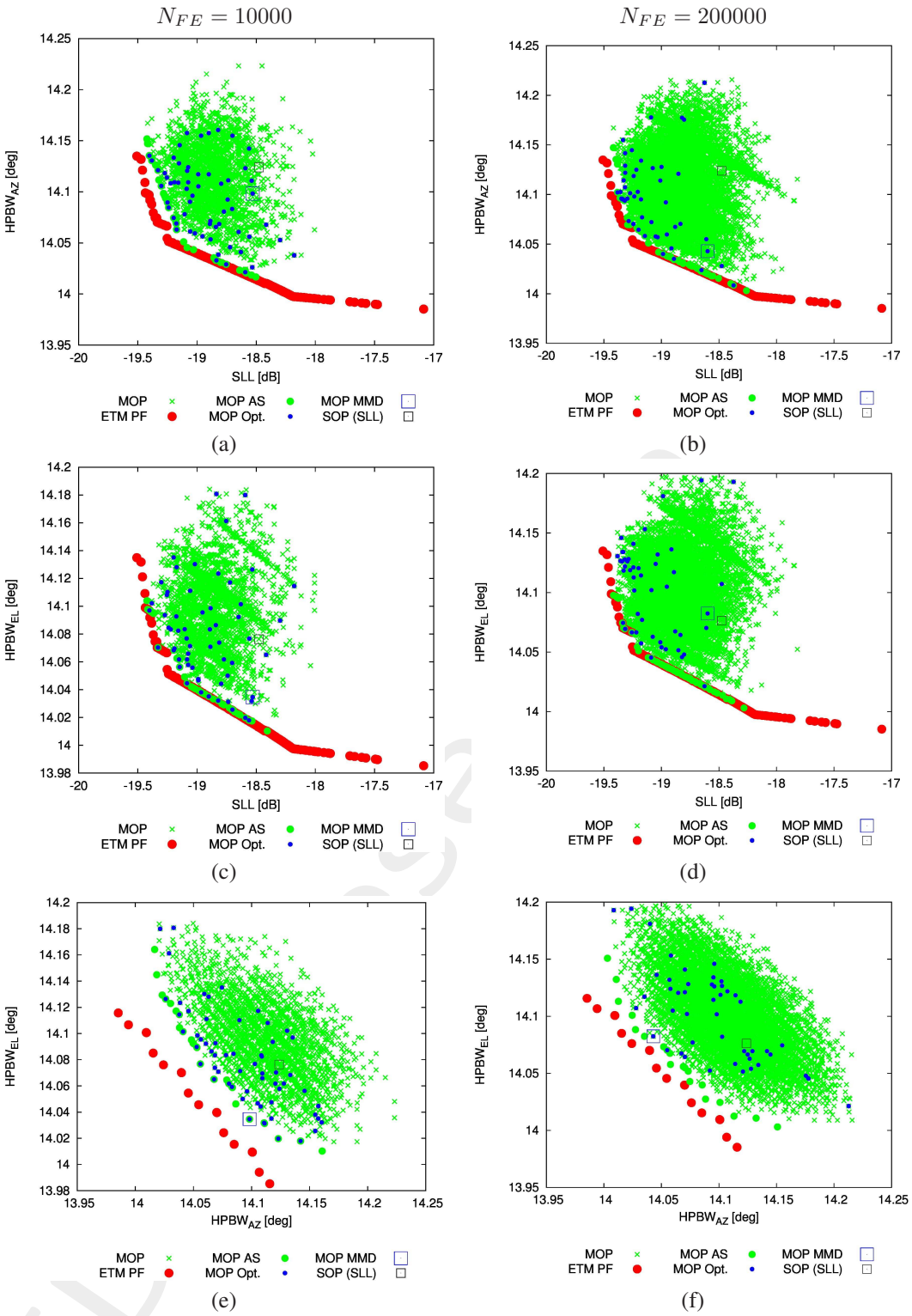


Figure 8: Exhaustive Pareto front as compared to the $MOP$ Approximation Set considering: $OBJ^{(1)} = SLL$ vs $OBJ^{(2)} = HPBW_{AZ}$ (a)(b), $OBJ^{(1)} = SLL$ vs $OBJ^{(3)} = HPBW_{EL}$(c)(d), $OBJ^{(2)} = HPBW_{AZ}$ vs $OBJ^{(3)} = HPBW_{EL}$(e)(f), for $N_{FE} = 10000$ and $N_{FE} = 200000$ fitness evaluations.

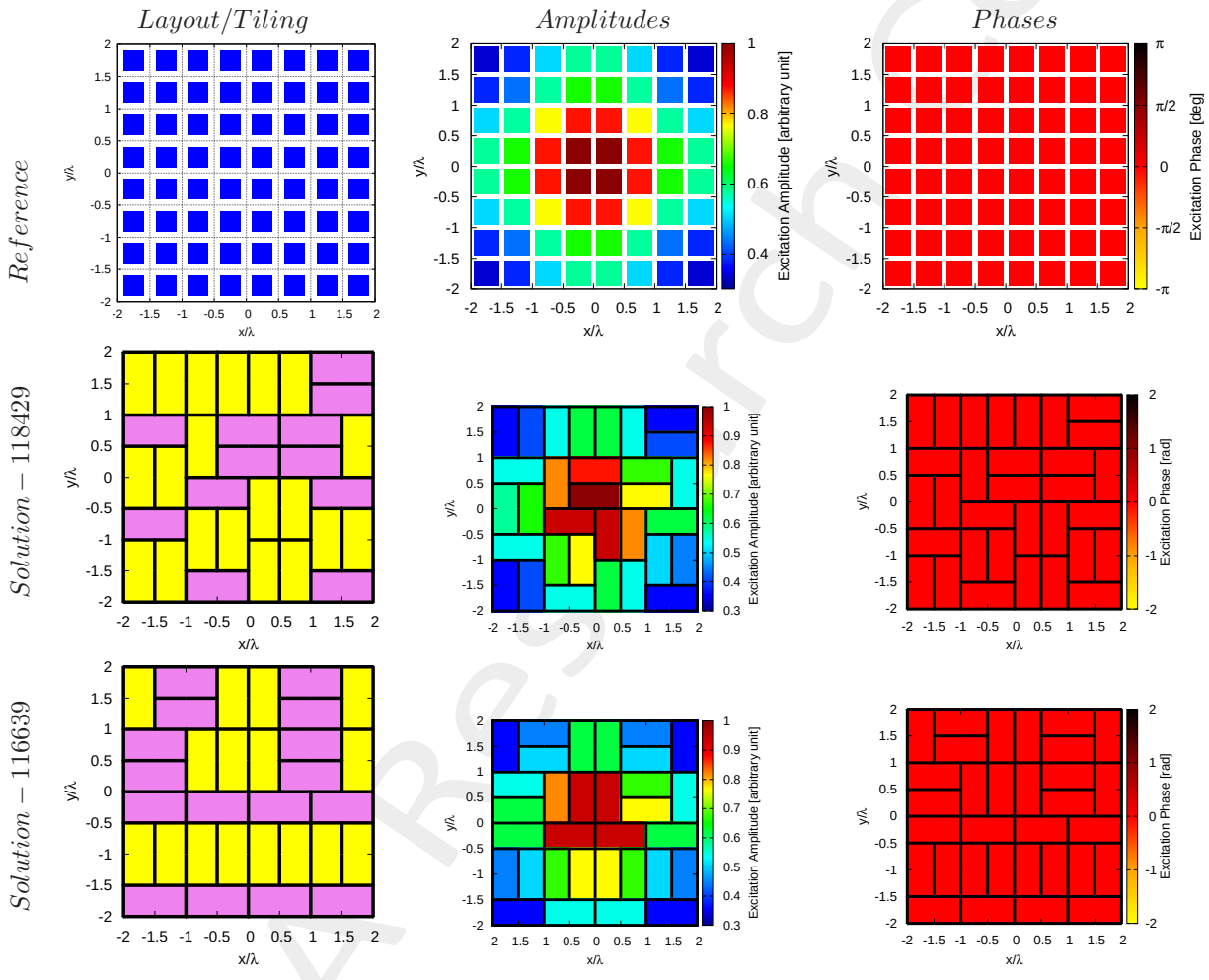


Figure 9: Tiling Configurations/Excitations.

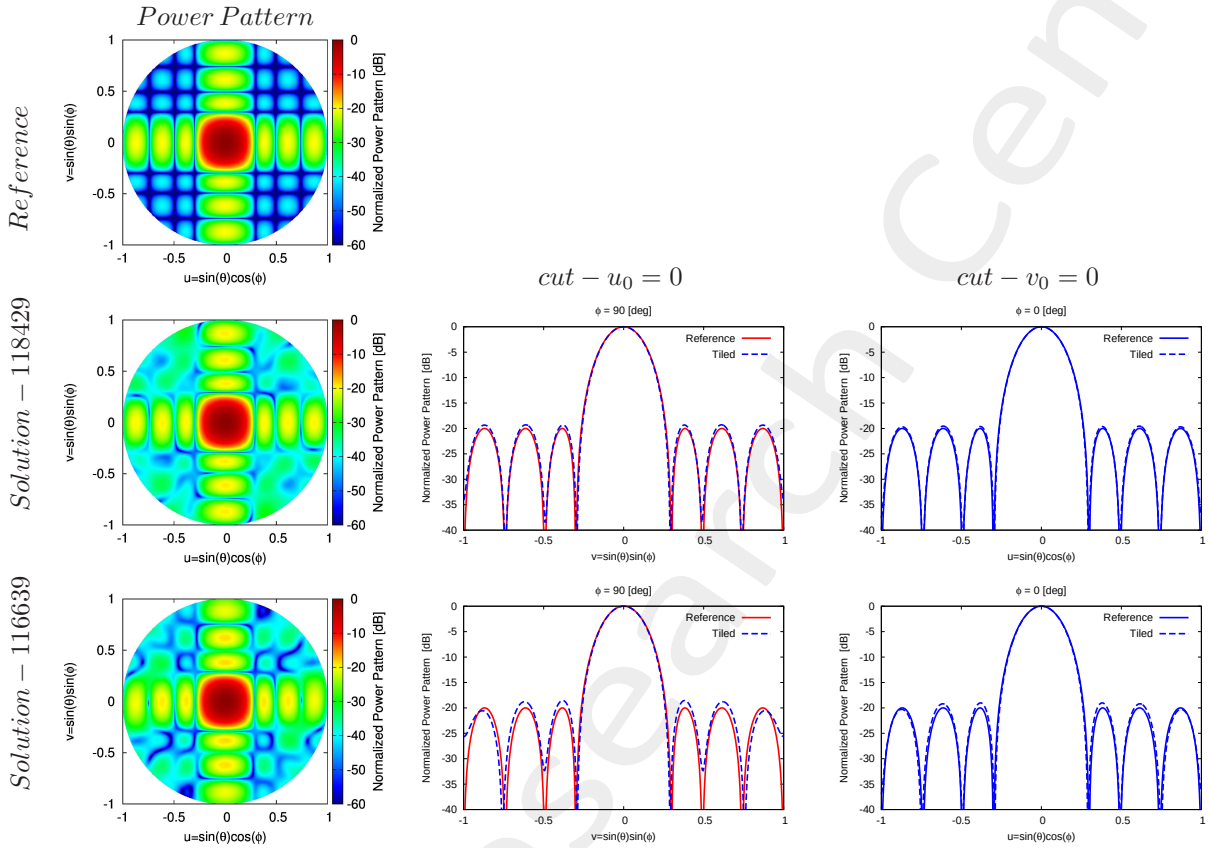


Figure 10: Power Patterns.

| | $SLL$ [dB] | $D$ [dBi] | $HPBW_{az}$ [deg] | $HPBW_{el}$ [deg] | $\Psi\,(T)$ |
|---|---|---|---|---|---|
| $Reference$ | $-20.00$ | 22.47 | 14.23 | 14.23 | – |
| $Solution-118429$ | $-19.28$ | 22.46 | 14.14 | 14.07 | – |
| $Solution-116639$ | $-18.56$ | 22.48 | 14.08 | 14.06 | – |

Table I: Pattern descriptors and fitness values for the presented solutions.

**OUTCOME:**

- Solution-118429 is an end-user selected solution
- Solution-116639.

### 3.2.1 ETM-MOP - CP Reference Excitations, Symmetric Mask, SLL = -30 [dB] - Mask Matching vs {SLL, D, HPBW}

**Reference Fully-Populated Array:**

- Number of Samples along $u$: $512$ $-2 < u < 2$
- Number of Samples along $v$: $512$ $-2 < v < 2$
- Steering $\theta$ Direction: $\theta_s = 0$
- Steering $\phi$ Direction: $\phi_s = 0$
- Tapering: CP Symmetric Mask
- Main Lobe Window Width along u: $MW_u = 0.30$ [u]
- Main Lobe Window Width along v: $MW_v = 0.59$ [v]
- Side Lobe levels: $SLL = -30.0$

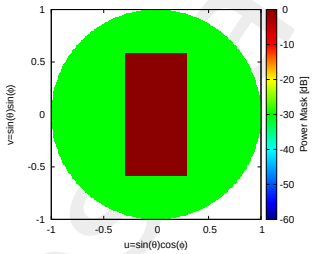


Figure 11: The power pattern mask used for the reference tapering optimization with $CP$.

**Cost Function:**

- $OBJ^{(1)} = SLL$
- $OBJ^{(2)} = HPBW_{AZ}$
- $OBJ^{(3)} = HPBW_{EL}$
- $OBJ^{(4)} = D$
- $OBJ^{(5)} = \int_{-1}^{1}\int_{-1}^{1}\left[M\left(u,v\right) - P\left(u,v;\underline{C}\right)\right]\mathcal{H}\left[P\left(u,v;\underline{C}\right) - M\left(u,v\right)\right]dudv$

## RESULTS

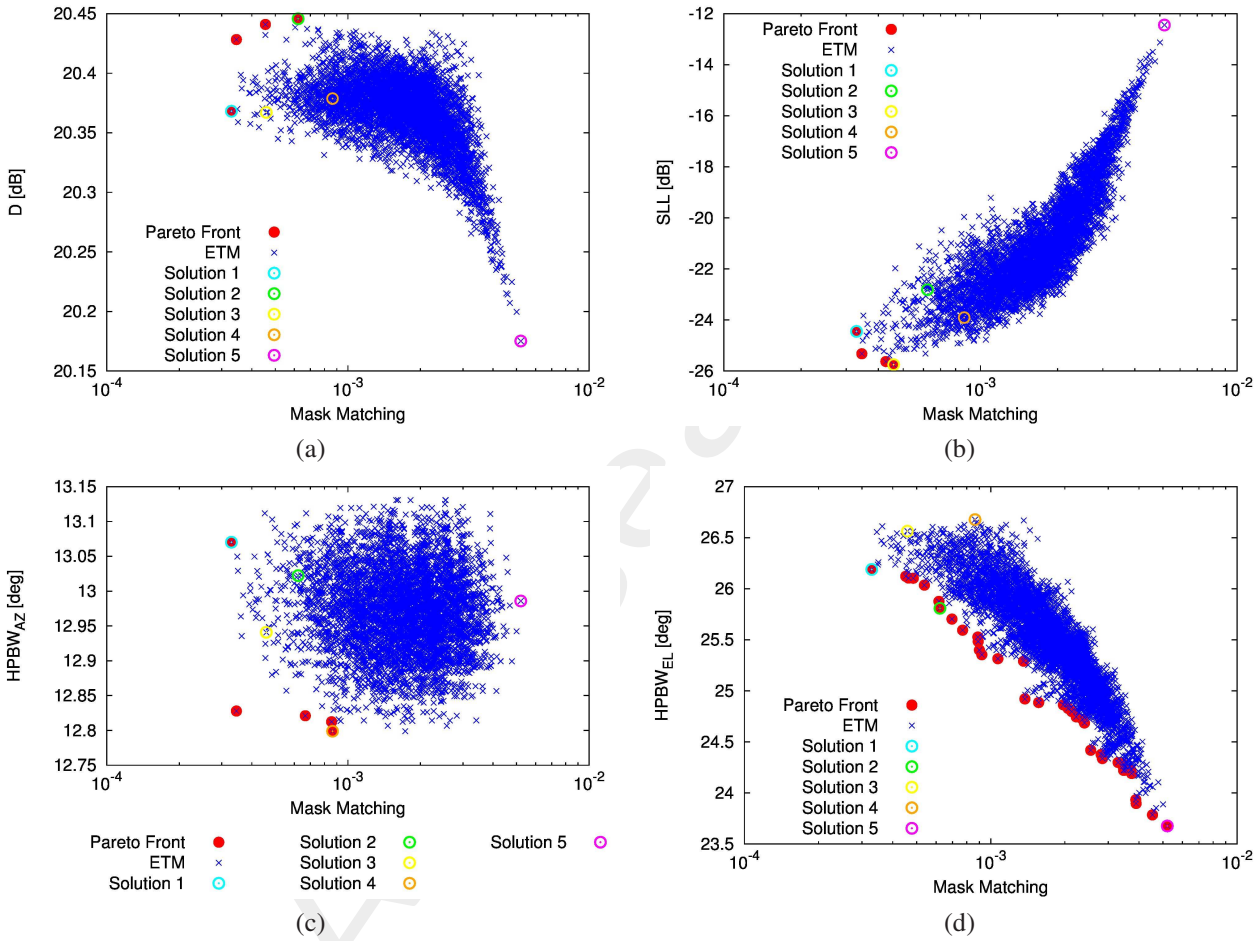


Figure 12: Pareto front of the $ETM$ soutions.

| | $Solution\,ID$ | $SLL$ [dB] | $D$ [dBi] | $HPBW_{az}$ [deg] | $HPBW_{el}$ [deg] | $Mask\,Matching$ |
|---|---|---|---|---|---|---|
| $Reference$ | – | $-30.00$ | 20.36 | 13.14 | 26.66 | 0.00 |
| $Solution-1$ | 8232 | $-24.45$ | 20.37 | 13.07 | 26.19 | $3.29\times10^{-4}$ |
| $Solution-2$ | 205 | $-22.81$ | 20.45 | 13.02 | 25.81 | $6.22\times10^{-4}$ |
| $Solution-3$ | 48 | $-25.75$ | 20.37 | 12.94 | 26.56 | $4.59\times10^{-4}$ |
| $Solution-4$ | 878 | $-23.91$ | 20.38 | 12.80 | 26.68 | $8.64\times10^{-4}$ |
| $Solution-5$ | 5948 | $-12.44$ | 20.18 | 12.99 | 23.68 | $5.21\times10^{-3}$ |

Table II: Pattern descriptors and fitness values for the presented solutions.

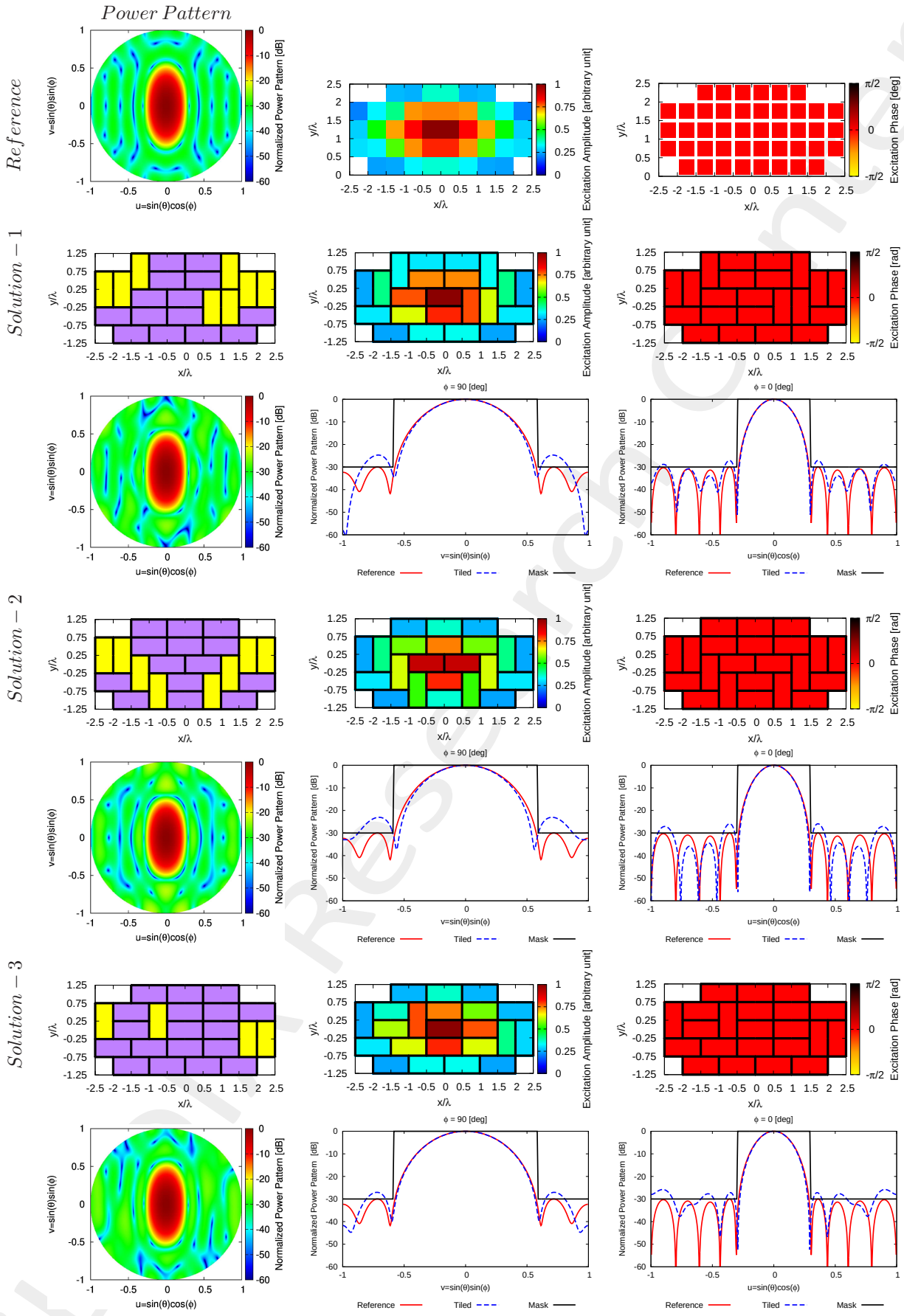


Figure 13: Power Patterns.

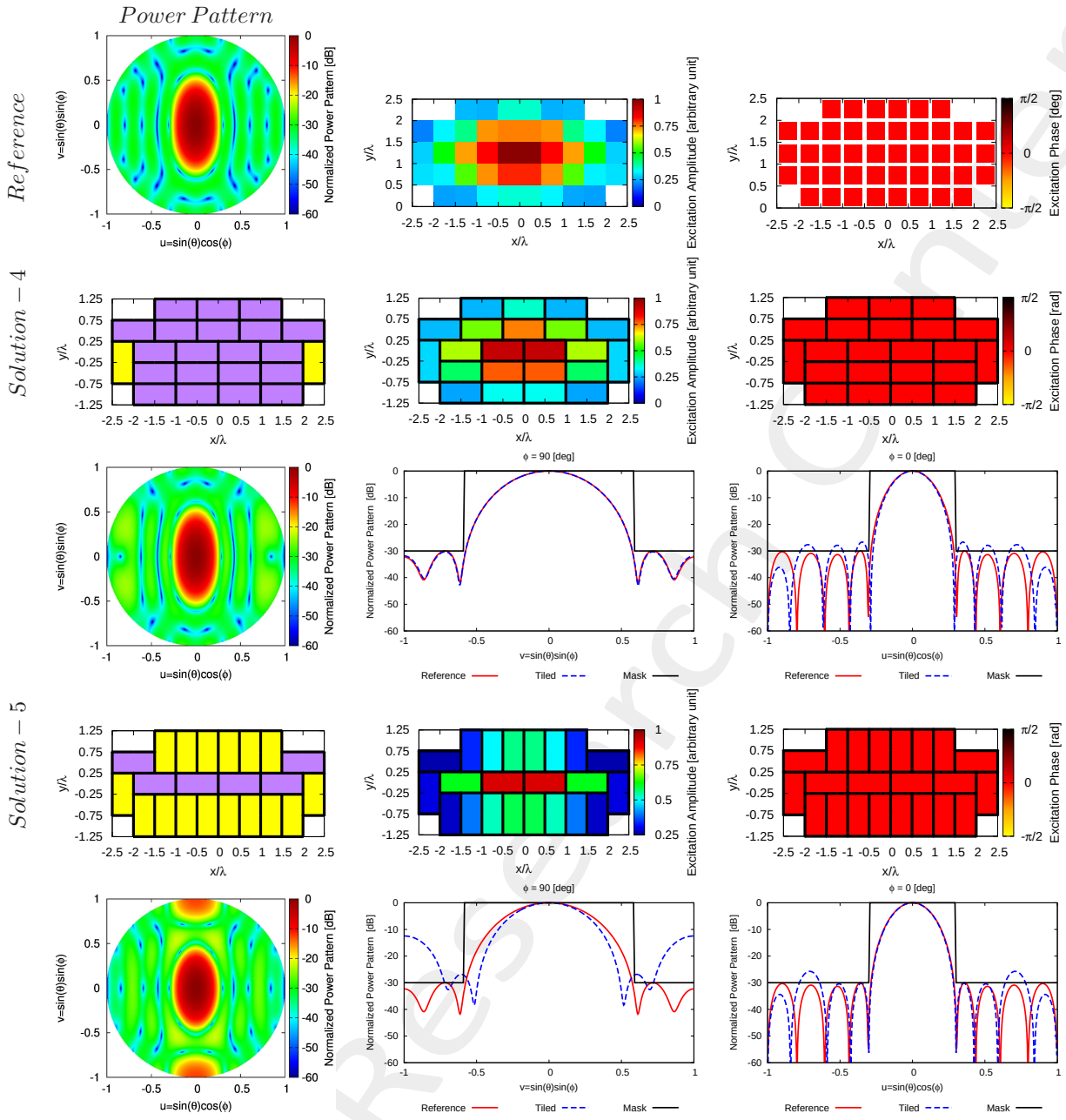


Figure 14: Power Patterns.

### 3.2.2 ETM-MOP - CP Reference Excitations, Symmetric Mask, SLL = -40 [dB] - Mask Matching vs {SLL, D, HPBW}

**Reference Fully-Populated Array:**

- Number of Samples along $u$: $512$ $-2 < u < 2$
- Number of Samples along $v$: $512$ $-2 < v < 2$
- Steering $\theta$ Direction: $\theta_s = 0$
- Steering $\phi$ Direction: $\phi_s = 0$
- Tapering: CP Symmetric Mask
- Main Lobe Window Width along u: $MW_u = 0.38$ [u]
- Main Lobe Window Width along v: $MW_v = 0.68$ [v]
- Side Lobe levels: $SLL = -40.0$

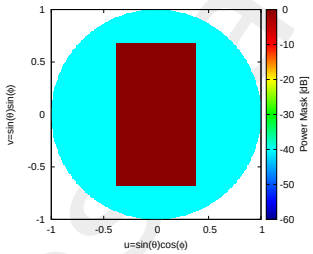


Figure 15: The power pattern mask used for the reference tapering optimization with $CP$.

**Cost Function:**

- $OBJ^{(1)} = SLL$
- $OBJ^{(2)} = HPBW_{AZ}$
- $OBJ^{(3)} = HPBW_{EL}$
- $OBJ^{(4)} = D$
- $OBJ^{(5)} = \int_{-1}^{1}\int_{-1}^{1}\left[M\left(u,v\right) - P\left(u,v;\underline{C}\right)\right]\mathcal{H}\left[P\left(u,v;\underline{C}\right) - M\left(u,v\right)\right]dudv$

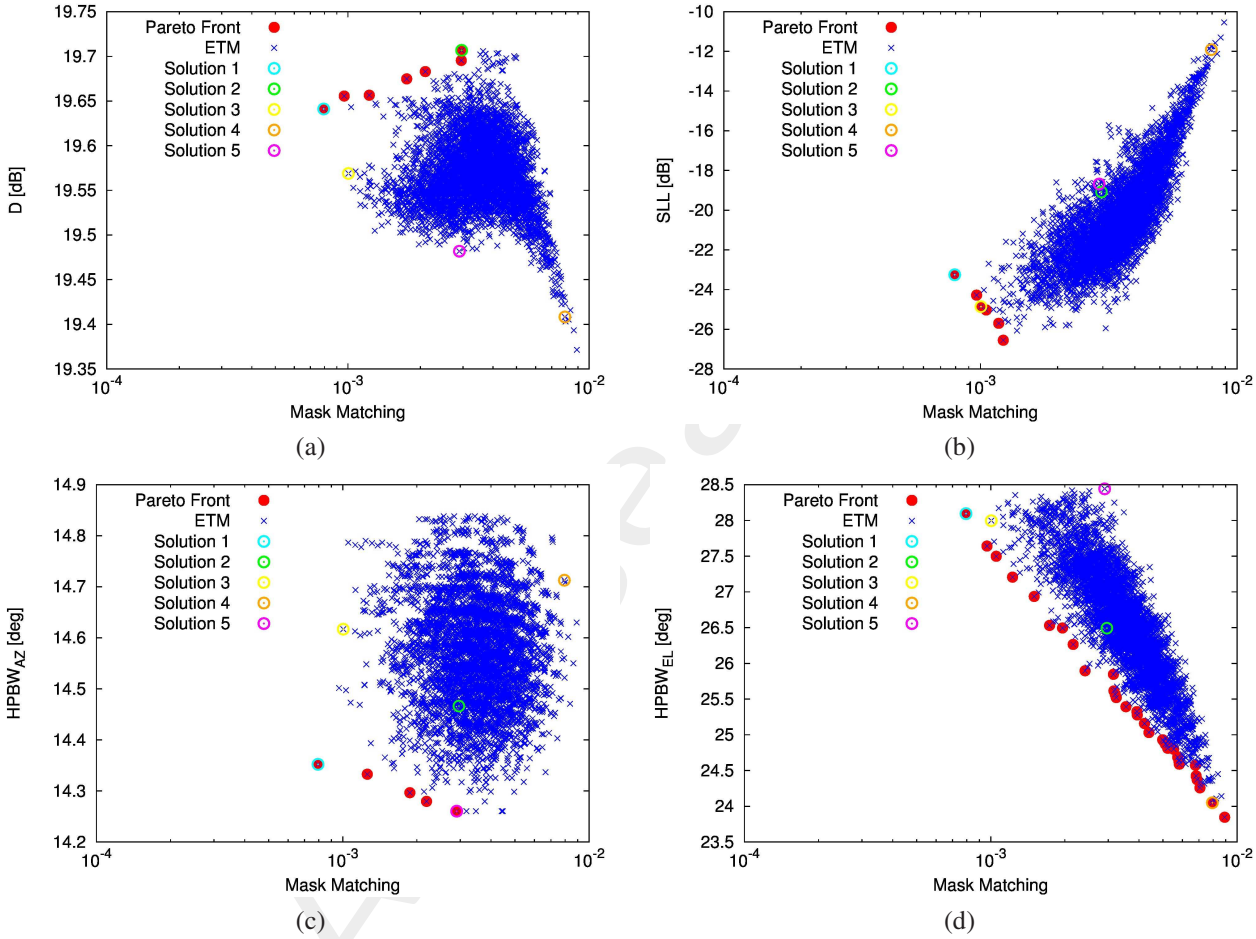


Figure 16: Pareto front of the $ETM$ soutions.

| | $Solution\,ID$ | $SLL$ [dB] | $D$ [dBi] | $HPBW_{az}$ [deg] | $HPBW_{el}$ [deg] | $Mask\,Matching$ |
|---|---|---|---|---|---|---|
| $Reference$ | – | $-39.84$ | 19.50 | 14.99 | 28.44 | 0.00 |
| $Solution-1$ | 911 | $-23.22$ | 19.64 | 14.35 | 28.10 | $7.94 \times 10^{-4}$ |
| $Solution-2$ | 7296 | $-19.08$ | 19.71 | 14.47 | 26.49 | $2.96 \times 10^{-3}$ |
| $Solution-3$ | 69 | $-24.86$ | 19.57 | 14.62 | 28.00 | $1.00 \times 10^{-3}$ |
| $Solution-4$ | 5670 | $-11.91$ | 19.41 | 14.71 | 24.05 | $7.94 \times 10^{-3}$ |
| $Solution-5$ | 626 | $-18.68$ | 19.48 | 14.26 | 28.44 | $2.90 \times 10^{-3}$ |

Table III: Pattern descriptors and fitness values for the presented solutions.

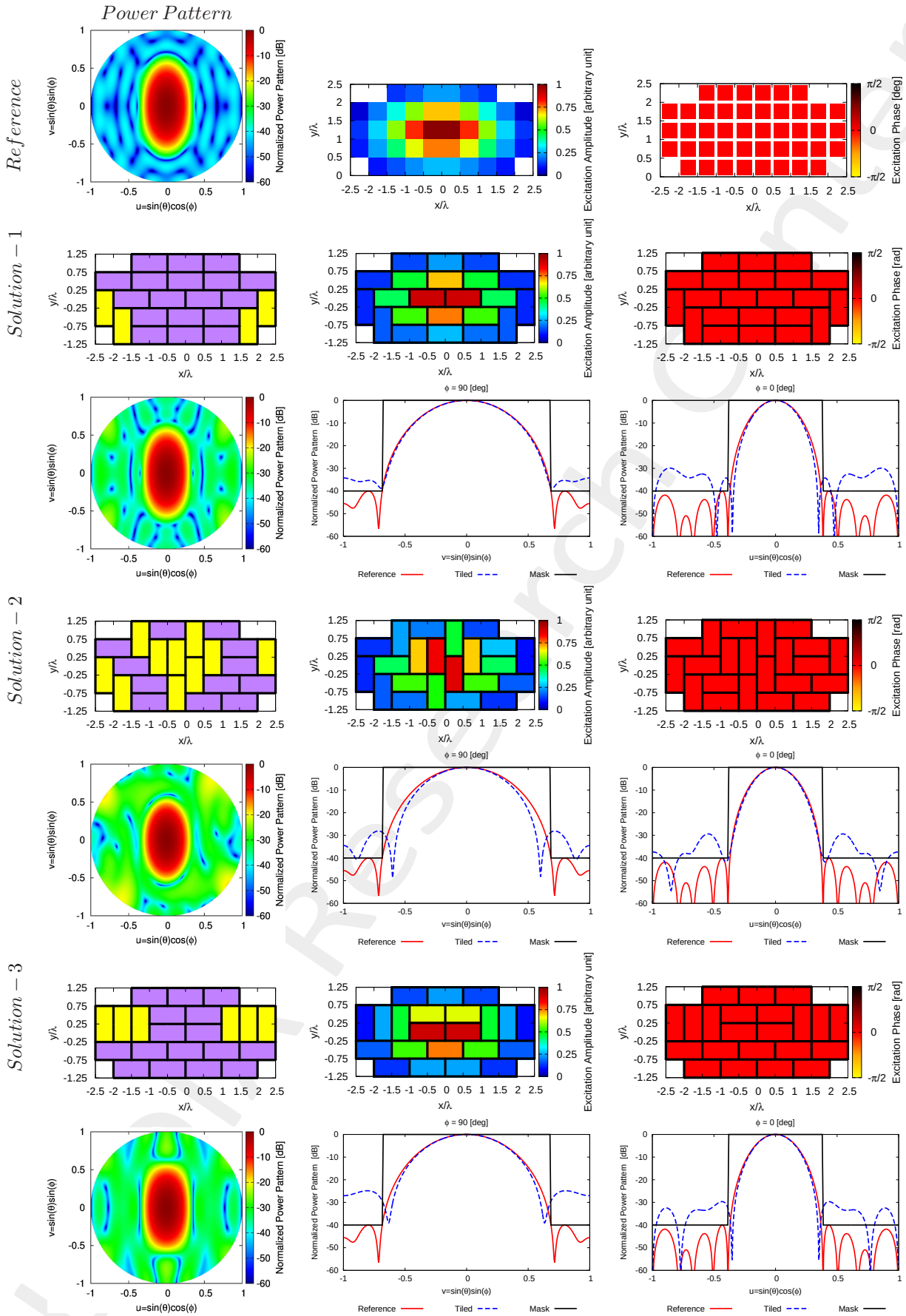


Figure 17: Power Patterns.

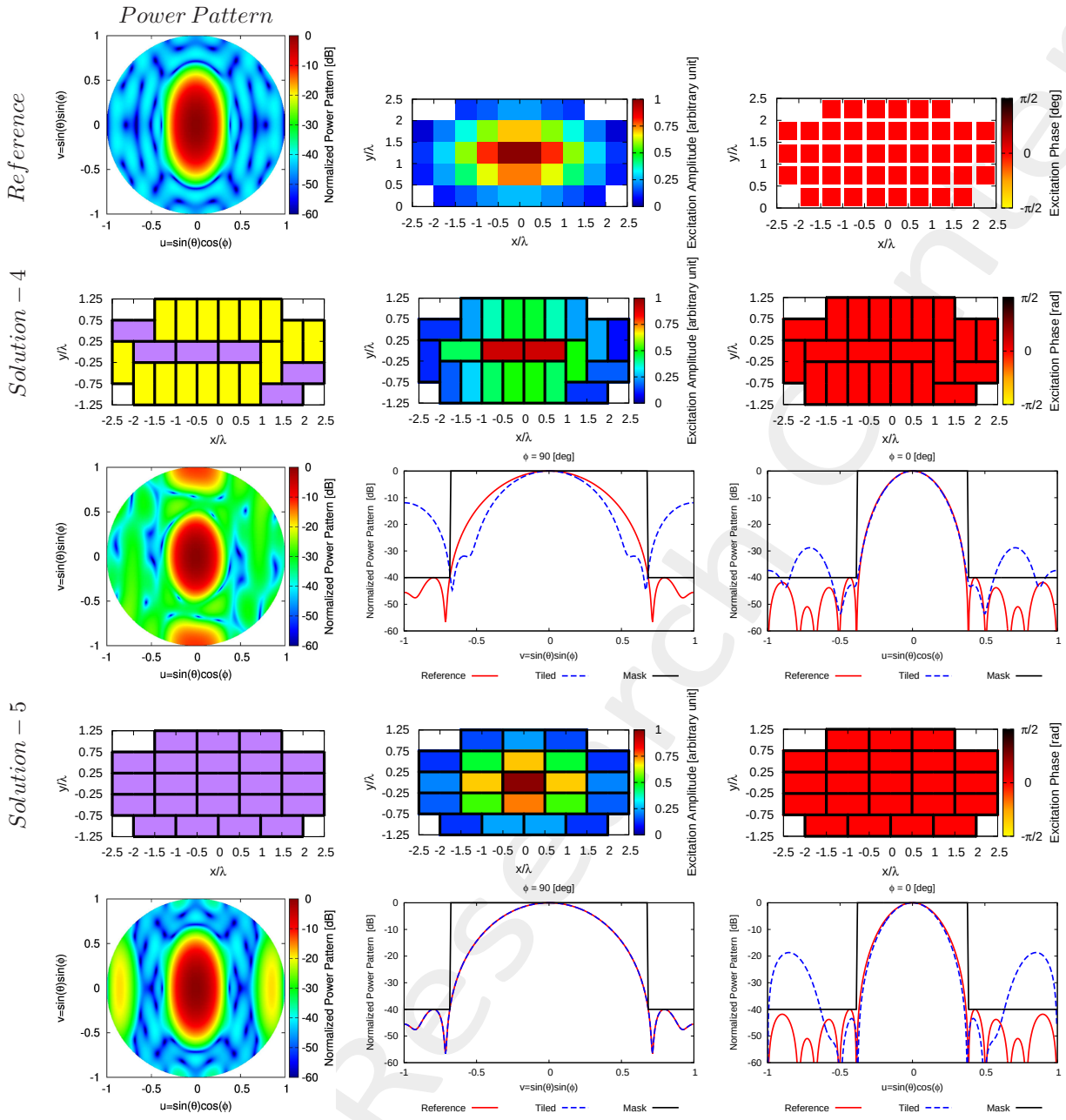


Figure 18: Power Patterns.

**More information on the topics of this document can be found in the following list of references.**

## References


[1] M. Salucci, G. Gottardi, N. Anselmi, and G. Oliveri, "Planar thinned array design by hybrid analytical-stochastic optimization," IET Microwaves, Antennas & Propagation, vol. 11, no. 13, pp. 1841-1845, Oct. 2017

[2] P. Rocca, N. Anselmi, A. Polo, and A. Massa, "Pareto-optimal domino-tiling of orthogonal polygon phased arrays," IEEE Trans. Antennas Propag., vol. 70, no. 5, pp. 3329-3342, May 2022.

[3] P. Rocca, N. Anselmi, A. Polo, and A. Massa, "An irregular two-sizes square tiling method for the design of isophoric phased arrays," IEEE Trans. Antennas Propag., vol. 68, no. 6, pp. 4437-4449, Jun. 2020.

[4] P. Rocca, N. Anselmi, A. Polo, and A. Massa, "Modular design of hexagonal phased arrays through diamond tiles," IEEE Trans. Antennas Propag., vol.68, no. 5, pp. 3598-3612, May 2020.

[5] N. Anselmi, L. Poli, P. Rocca, and A. Massa, "Design of simplified array layouts for preliminary experimental testing and validation of large AESAs," IEEE Trans. Antennas Propag., vol. 66, no. 12, pp. 6906-6920, Dec. 2018.

[6] N. Anselmi, P. Rocca, M. Salucci, and A. Massa, "Contiguous phase-clustering in multibeam-on-receive scanning arrays" IEEE Trans. Antennas Propag., vol. 66, no. 11, pp. 5879-5891, Nov. 2018.

[7] G. Oliveri, G. Gottardi, F. Robol, A. Polo, L. Poli, M. Salucci, M. Chuan, C. Massagrande, P. Vinetti, M. Mattivi, R. Lombardi, and A. Massa, "Co-design of unconventional array architectures and antenna elements for 5G base station," IEEE Trans. Antennas Propag., vol. 65, no. 12, pp. 6752-6767, Dec. 2017.

[8] N. Anselmi, P. Rocca, M. Salucci, and A. Massa, "Irregular phased array tiling by means of analytic schemata-driven optimization," IEEE Trans. Antennas Propag., vol. 65, no. 9, pp. 4495-4510, September 2017.

[9] N. Anselmi, P. Rocca, M. Salucci, and A. Massa, "Optimization of excitation tolerances for robust beamforming in linear arrays" IET Microwaves, Antennas & Propagation, vol. 10, no. 2, pp. 208-214, 2016.

[10] P. Rocca, R. J. Mailloux, and G. Toso, "GA-Based optimization of irregular sub-array layouts for wideband phased arrays desig," IEEE Antennas and Wireless Propag. Lett., vol. 14, pp. 131-134, 2015.

[11] P. Rocca, M. Donelli, G. Oliveri, F. Viani, and A. Massa, "Reconfigurable sum-difference pattern by means of parasitic elements for forward-looking monopulse radar," IET Radar, Sonar & Navigation, vol 7, no. 7, pp. 747-754, 2013.

[12] M. Salucci, G. Oliveri, M. A. Hannan, and A. Massa, âSystem-by-design paradigm-based synthesis of complex systems: The case of spline-contoured 3D radomes,â IEEE Antennas and Propagation Magazine â Special Issue on âArtificial Intelligence in Electromagnetics,â, vol. 64, no. 1, pp. 72-83, Feb. 2022.

[13] G. Oliveri, A. Gelmini, A. Polo, N. Anselmi, and A. Massa, "System-by-design multi-scale synthesis of task-oriented reflectarrays," IEEE Trans. Antennas Propag., vol. 68, no. 4, pp. 2867-2882, Apr. 2020.

[14] N. Anselmi, L. Poli, P. Rocca, and A. Massa, "Design of simplified array layouts for preliminary experimental testing and validation of large AESAs," IEEE Trans. Antennas Propag., vol. 66, no. 12, pp. 6906-6920, Dec. 2018.

[15] M. Salucci, F. Robol, N. Anselmi, M. A. Hannan, P. Rocca, G. Oliveri, M. Donelli, and A. Massa, "S-Band spline-shaped aperture-stacked patch antenna for air traffic control applications," IEEE Tran. Antennas Propag., vol. 66, no. 8, pp. 4292-4297, Aug. 2018.

[16] M. Salucci, L. Poli, A. F. Morabito, and P. Rocca, "Adaptive nulling through subarray switching in planar antenna arrays," Journal of Electromagnetic Waves and Applications, vol. 30, no. 3, pp. 404-414, February 2016

[17] T. Moriyama, L. Poli, and P. Rocca, "Adaptive nulling in thinned planar arrays through genetic algorithms" IEICE Electronics Express, vol. 11, no. 21, pp. 1-9, Sep. 2014.

[18] L. Poli, P. Rocca, M. Salucci, and A. Massa, "Reconfigurable thinning for the adaptive control of linear arrays," IEEE Trans. Antennas Propag., vol. 61, no. 10, pp. 5068-5077, Oct. 2013.

[19] P. Rocca, L. Poli, G. Oliveri, and A. Massa, "Adaptive nulling in time-varying scenarios through time-modulated linear arrays," IEEE Antennas Wireless Propag. Lett., vol. 11, pp. 101-104, 2012.

[20] L. Poli, D. Masotti, M. A. Hannan, A. Costanzo, and P. Rocca, "Codesign of switching sequence and diode parameters for multiple pattern optimization in time-modulated arrays," IEEE Antennas Wireless Propag. Lett. â Special Issue on âSpace-Time Modulated Antennas and Materialsâ, vol. 19, no. 11, pp. 1852-1856, Nov. 2020.

[21] P. Rocca, F. Yang, L. Poli, and S. Yang, "Time-modulated array antennas - Theory, techniques, and applications" Journal of Electromagnetic Waves and Applications, vol. 33, no. 12, pp. 1503-1531, Jun. 2019.

[22] L. Poli, P. Rocca, G. Oliveri, M. Chuan, C. Mazzucco, S. Verzura, R. Lombardi, and A. Massa, "Advanced pulse sequence design in time-modulated arrays for cognitive radio," IEEE Antennas Wireless Propagat. Lett., vol. 17, no. 5, pp. 898-902, May 2018.

[23] P. Rocca, G. Oliveri, R. J. Mailloux, and A. Massa, "Unconventional phased array architectures and design Methodologies - A review," Proceedings of the IEEE - Special Issue on 'Phased Array Technologies', Invited Paper, vol. 104, no. 3, pp. 544-560, March 2016.

[24] L. Poli, P. Rocca, G. Oliveri, and A. Massa, "Failure correction in time-modulated linear arrays," IET Radar, Sonar & Navigation, vol. 8, no. 3, pp. 195-201, 2014.

[25] L. Poli, T. Moriyama, and P. Rocca, "Pulse splitting for harmonic beamforming in time-modulated linear arrays," International Journal of Antennas and Propagation, vol. 2014, pp. 1-9, 2014.

[26] P. Rocca, Q. Zhu, E.T. Bekele, S. Yang, A. Massa, "4D arrays as enabling technology for cognitive radio systems" IEEE Trans. Antennas Propag., vol. 62, no. 3. pp. 1102-1116, Mar. 2014.

[27] E. T. Bekele, L. Poli, M. D'Urso, P. Rocca, and A. Massa, "Pulse-shaping strategy for time modulated arrays - Analysis and design," IEEE Trans. Antennas Propag., vol. 61, no. 7, pp. 3525-3537, July 2013.

[28] P. Rocca, M. D'Urso, and L. Poli, An iterative approach for the synthesis of optimized sparse time-modulated linear arrays," Progress In Electromagnetics Research B, vol. 55, pp. 365-382, 2013.

[29] P. Rocca, L. Poli, G. Oliveri, and A. Massa, "Adaptive nulling in time-varying scenarios through time-modulated linear arrays," IEEE Antennas Wireless Propag. Lett., vol. 11, pp. 101-104, 2012.

[30] P. Rocca, L. Poli, and A. Massa, "Instantaneous directivity optimization in time-modulated array receivers," IET Microwaves, Antennas & Propagation, vol. 6, no. 14, pp. 1590-1597, Nov. 2012.

[31] P. Rocca, L. Poli, L. Manica, and A. Massa, "Synthesis of monopulse time-modulated planar arrays with controlled sideband radiation," IET Radar, Sonar & Navigation, vol. 6, no. 6, pp. 432-442, 2012.

[32] L. Poli, P. Rocca, and A. Massa, "Sideband radiation reduction exploiting pattern multiplication in directive time-modulated linear arrays," IET Microwaves, Antennas & Propagation, vol. 6, no. 2, pp. 214-222, 2012.

[33] P. Rocca, L. Poli, A. Polo, and A. Massa, "Optimal excitation matching strategy for sub-arrayed phased linear arrays generating arbitrary shaped beams," IEEE Trans. Antennas Propag., vol. 68, no. 6, pp. 4638-4647, Jun. 2020.

[34] G. Oliveri, G. Gottardi and A. Massa, "A new meta-paradigm for the synthesis of antenna arrays for future wireless communications," IEEE Trans. Antennas Propag., vol. 67, no. 6, pp. 3774-3788, Jun. 2019.

[35] P. Rocca, M. H. Hannan, L. Poli, N. Anselmi, and A. Massa, "Optimal phase-matching strategy for beam scanning of sub-arrayed phased arrays," IEEE Trans. Antennas and Propag., vol. 67, no. 2, pp. 951-959, Feb. 2019.

[36] N. Anselmi, P. Rocca, M. Salucci, and A. Massa, "Contiguous phase-clustering in multibeam-on-receive scanning arrays" IEEE Trans. Antennas Propag., vol. 66, no. 11, pp. 5879-5891, Nov. 2018.

[37] L. Poli, G. Oliveri, P. Rocca, M. Salucci, and A. Massa, "Long-Distance WPT Unconventional Arrays Synthesis" Journal of Electromagnetic Waves and Applications, vol. 31, no. 14, pp. 1399-1420, Jul. 2017.

[38] G. Gottardi, L. Poli, P. Rocca, A. Montanari, A. Aprile, and A. Massa, "Optimal Monopulse Beamforming for Side-Looking Airborne Radars," IEEE Antennas Wireless Propag. Lett., vol. 16, pp. 1221-1224, 2017.

[39] G. Oliveri, M. Salucci, and A. Massa, "Synthesis of modular contiguously clustered linear arrays through a sparseness-regularized solver," IEEE Trans. Antennas Propag., vol. 64, no. 10, pp. 4277-4287, Oct. 2016.

[40] P. Rocca, G. Oliveri, R. J. Mailloux, and A. Massa, "Unconventional phased array architectures and design Methodologies - A review" Proceedings of the IEEE = Special Issue on 'Phased Array Technologies', Invited Paper, vol. 104, no. 3, pp. 544-560, March 2016.

[41] P. Rocca, M. D'Urso, and L. Poli,"Advanced strategy for large antenna array design with subarray-only amplitude and phase contr," IEEE Antennas and Wireless Propag. Lett., vol. 13, pp. 91-94, 2014.